Oxygenation of monolayer gallium monochalcogenides: Design of two-dimensional ternary Ga$_2X$O structures (X = S, Se, Te)

M. Demirtas,[1,2] B. Ozdemir ,[1] Y. Mogulkoc,[3] and E. Durgun [1,*]

[1]*UNAM—National Nanotechnology Research Center and Institute of Materials Science and Nanotechnology, Bilkent University, Ankara 06800, Turkey*
[2]*Department of Physics, Kafkas University, Kars 36100, Turkey*
[3]*Department of Physics Engineering, Faculty of Engineering, Ankara University, Tandogan, Ankara 06100, Turkey*

The possibility of breaking structural symmetry with realization of Janus monolayers offers new possibilities in the field of two-dimensional (2D) materials, and various ternary systems including the class of group-III monochalcogenides have been suggested. However, interaction of oxygen was shown to modify optoelectronic properties of gallium monochalcogenides, and design of ternary systems with oxygen as a third component has not been considered yet. In this paper, we design and investigate 2D Ga$_2X$O (X = S, Se, Te) systems by using first-principles calculations. Phonon spectra analysis and molecular dynamics simulations indicate that while Ga$_2$SO and Ga$_2$SeO are stable even at high temperatures Ga$_2$TeO is dynamically unstable. Inclusion of oxygen makes Ga$_2$SO and Ga$_2$SeO less brittle when compared to their binary constituents. While GaX monolayers have indirect band gaps, Ga$_2$SO and Ga$_2$SeO become direct band-gap semiconductors and the band gap can be further tuned by tensile/compressive strain. Additionally, depending on the type of the system, strong optical absorption within the infrared, visible, and/or ultraviolet region is also predicted. Finally, structural and electronic properties of bilayers of Ga$_2X$O are examined and compared with monolayers. Our results not only predict stable 2D ternary Ga$_2X$O structures but also suggest them as promising materials for optoelectronic applications.

I. INTRODUCTION

The discovery of graphene has initiated an extensive research being carried out to manufacture and design new classes of two-dimensional (2D) materials [1–3]. In this quest many 2D systems beyond graphene have been realized, and within these classes there has been a surge of interest in the family of group-III monochalcogenides with formula MX (M = B, Ga, Al, In and X = O, S, Se, Te) due to their remarkable properties which make them useful in various applications [4]. To date, 2D GaS [5–7], GaSe [8,9], GaTe [10,11], and InSe [12,13] have been synthesized and have been extensively examined [14]. The intriguing electrical, optical, and mechanical properties of GaS monolayers have been revealed and they have been suggested as an ideal material for optoelectronic applications [15,16]. High-responsive photodetectors based on GaS and GaSe monolayers have been reported [7,8] and these systems have been proposed as potential water splitting catalysts since their band edges are aligned with the redox potential of water [17]. Heterostructures of GaS and GaSe with type-II band alignment which enables physical separation of excitons have been predicted [18]. In addition to fabricated systems, all dynamically stable configurations of MX monolayers have been examined and they have been classified as indirect semiconductors with band

gaps between 1.21 and 6.24 eV covering a wide range of the optical spectrum [14]. It has been also noted that MO monolayers behave significantly different than the rest of the MX systems [14]. In a similar manner, it has been shown that the electronic and topological properties of single layer MXs [19] and their ultrathin films [20] can be tuned by oxygen functionalization or oxidation at ambient conditions.

The development of 2D materials is not limited by monoelemental or binary systems but they have been followed by fabrication of ternary structures in alignment with advancement in experimental techniques. Lu *et al.* have reported the production of ternary MoSSe monolayers by replacing all of the S atoms at one side of MoS$_2$ by Se atoms [21]. By this way, the out-of-plane mirror symmetry is broken, resulting in new properties different than the binary counterpart. Subsequently, the Janus SMoSe monolayer has been synthesized by replacing one layer of Se atoms of MoSe$_2$ with S atoms via controlled sulfurization [22]. The resulting structure has characteristic Raman peaks differentiating it from the MoS$_2$ and MoSe$_2$ monolayers. These efforts are not restricted to transition-metal dichalcogenides but have also been extended to different classes including the ternary group-III monochalcogenides. The Janus monolayer of In$_2$SSe has been predicted recently [23] and an indirect-direct band-gap transition due to broken vertical symmetry has been reported. The other ternary derivatives of group-III monochalcogenides have been also theoretically investigated and they have been suggested as piezoelectric materials with high piezoelectric
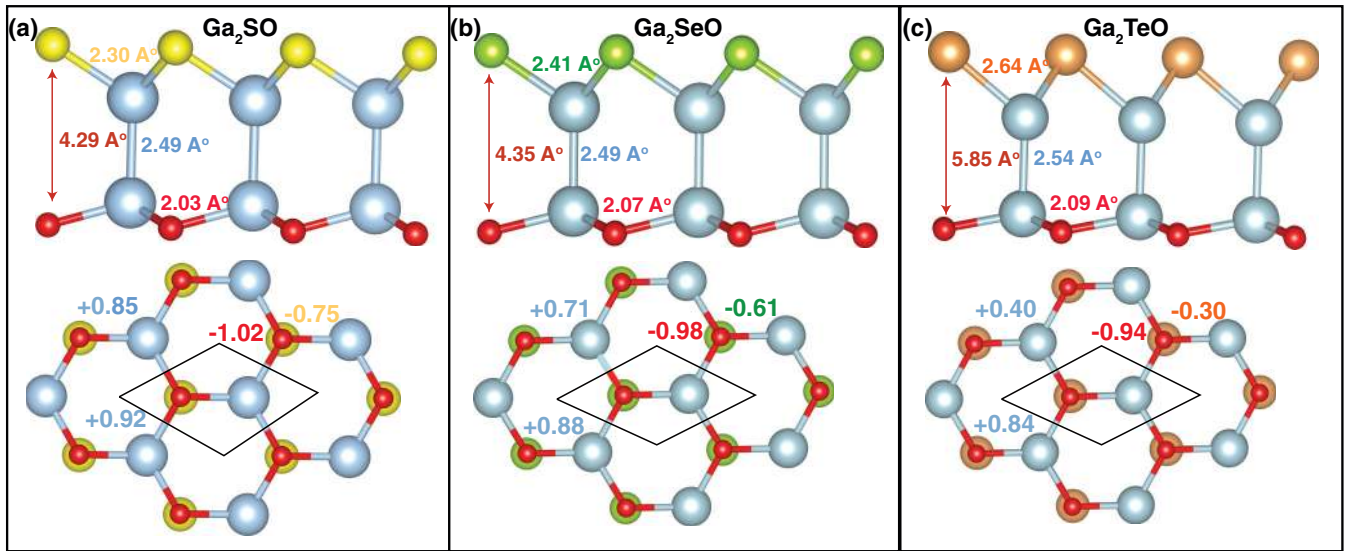
*durgun@unam.bilkent.edu.tr

FIG. 1. The side and top views of (a) Ga_2SO, (b) Ga_2SeO, and (c) Ga_2TeO monolayers. Ga, S, Se, Te, and O atoms are shown with blue, yellow, green, orange, and red spheres, respectively. The bond length between Ga-Ga (d_{Ga-Ga}), Ga-O (d_{Ga-O}), Ga-X d_{Ga-X}), and thickness (d_{X-O}) (side view) and donated/accepted ($+/-$) charges (top view) are also represented with relevant color codes.

coefficients [24]. Finally, Bui *et al.* examined the structural, electronic, and optical properties of Janus Ga_2SSe, Ga_2STe, and Ga_2SeTe monolayers [25] and compared the obtained electronic band gaps with their binary analogs.

On the other hand, while it has been shown that MX monolayers and thin films exhibit different characteristics with oxygen functionalization, their possible ternary structures with inclusion of oxygen have not been studied yet. With this in mind, in this paper we examine the structural, vibrational, electronic, and optical properties of mono- and bilayers of Ga_2XO ($X = S$, Se, Te) by first-principles methods to reveal the effect of oxygenation. First, the ground-state structures of Ga_2XO monolayers are obtained and their dynamical stabilities are tested by phonon spectrum analysis and molecular dynamic calculations. Next, the electronic properties are investigated and the variation of the band gap under strain is also considered. In relation to electronic structure, the optical response is studied following the calculation of the complex dielectric function. Finally, the structural and electronic properties of the bilayers are analyzed by taking into account all possible stackings.

II. METHOD

All first-principles calculations were carried out within the framework of density functional theory (DFT) implemented in the Vienna Ab initio Simulation Package [26–29]. The generalized gradient approximation with Perdew-Burke-Ernzerhof (GGA-PBE) formalism [30] was chosen to describe the exchange-correlation functional. The projected augmented wave method [31] with a kinetic-energy cutoff of 530 eV was used for element potentials. The Brillouin zone was sampled with a $16 \times 16 \times 1$ k-point mesh centered at the Γ point [32]. The random-phase approximation [33] with a $24 \times 24 \times 1$ k-point mesh was adopted to calculate the optical response. Local-field effects were accounted for the exchange-correlation potential. The linear response of the system to the

light-matter interaction is described by the complex dielectric function, $\epsilon(\omega) = \epsilon_1(\omega) + i\epsilon_2(\omega)$, where the Kramers-Kronig relation is applied to obtain the real and imaginary parts by taking into account the dielectric screening in 2D systems [34–37]. In addition to interband transitions, intraband transitions for metallic systems were also taken into account by calculating the plasma frequency. The structures were optimized until the energy difference between two consecutive steps was less than 10^{-5} eV and the force on the atoms was smaller than 0.01 eV/Å. A vacuum space was set to $\approx$15 Å, which was tested to be sufficient to prevent artificial interactions (i.e., a polarization induced electrostatic field in the vacuum region [38,39]) between images along the nonperiodic direction (see Supplemental Material [40]). Phonon dispersions were calculated by using a small displacement method implemented in the PHONOPY package [41]. Since the GGA-PBE formalism tends to underestimate the electronic band gaps, the Heyd-Scuseria-Ernzerhof (HSE06) hybrid functional approach was employed to obtain a more accurate electronic structure [42]. An empirical correction method of Grimme (DFT-D2) was applied to describe van der Waals (vdW) interactions [43]. The charges on the atoms were calculated by using the Bader charge technique [44].

III. RESULTS AND DISCUSSION

A. Structural properties and stability

To construct Janus Ga_2XO ($X = S$, Se, and Te) monolayers, either side of GaX consisting of X atoms is substituted with O atoms yielding three different structures (Ga_2SO, Ga_2SeO, and Ga_2TeO) as shown in Fig. 1. Similar to their binary counterparts, ternary systems have four covalently bonded atomic planes in which Ga layers are sandwiched between O and X atoms and hexagonal symmetry is retained. As listed in Table I, the optimized lattice constants (a) of Ga_2XO elongate down the chalcogen group and obtained values lie within those of binary analogs. In a similar manner, the bond

TABLE I. The lattice constant (a), cohesive energy per atom (E_C), energy band gap at the level of GGA-PBE (E_g^{PBE}) and HSE06 (E_g^{HSE}), Poisson's ratio (ν), in-plane stiffness (Y_{2D}), Young modulus Y, and electronegativity difference between Ga and X atoms ($\Delta\chi$, in Pauli scale). Metallic systems are denoted with M.

Type	a (Å)	E_C (eV/atom)	E_g^{PBE} (eV)	E_g^{HSE} (eV)	ν	Y_{2D} (J/m^2)	Y (GPa)	$\Delta\chi$
GaO	3.13	4.43	1.50	2.59	0.38	106	208	1.63
GaS	3.64	3.56	2.36	3.26	0.24	71	108	0.77
GaSe	3.82	3.37	1.78	2.64	0.24	58	86	0.74
GaTe	4.14	2.89	1.42	2.08	0.22	48	66	0.29
Ga$_2$SO	3.38	3.88	1.28	2.11	0.30	92	155	0.77
Ga$_2$SeO	3.47	3.62	0.39	1.03	0.32	80	134	0.74
Ga$_2$TeO	3.54	3.30	M	M	0.39	44	69	0.29

length between Ga and X/O atoms (d_{Ga-X}, d_{Ga-O}) and thickness (d_{X-O}) also increase with the size of X atoms as represented in Fig. 1. It should be noted that in addition to ideal geometries possible structural modifications that can arise from broken symmetry are also taken into account, however no distortions and/or structural phase transitions are obtained.

The cohesive energy per atom (E_C) of each structure is calculated with the following formula:

$$E_C = [N_{Ga}E_{Ga} + N_X E_X + N_O E_O - E_{Ga_2XO}]/(N_{Ga} + N_X + N_O) \quad (1)$$

where E_{Ga_2XO} represents the total energy of the Ga$_2X$O monolayer; E_{Ga}, E_X, and E_O are the single atom energies of Ga, X, and O elements, respectively, and N_{Ga}, N_X, and N_O are the number of corresponding elements in the unit cell. In parallel with the elongation of the bond length which indicates weakening of the bonds, E_C decreases down the chalcogen group as summarized in Table I. The obtained values are in between those of binary constituents (GaX and GaO) [14]. The trend can also be correlated with the average charge donated (accepted) by Ga (X and O) atoms as shown in Fig. 1. As the charge transfer depends on the electronegativity difference ($\Delta\chi$) between Ga and X atoms which decreases

from the O atom to the Te atom, the charge accepted by O is higher than all other chalcogen atoms. The asymmetry in charge transfer affects both the stability (see below) and physical properties of ternary systems.

Following the structural optimization, vibrational frequency analysis [Fig. 2(a)] is performed to test the dynamical stability of the considered structures. While all phonon modes of Ga$_2$SO and Ga$_2$SeO are positive, implying the dynamical stability at low temperature, the *ZA* mode of Ga$_2$TeO is imaginary, indicating that the structure is unstable. In addition to stability, a decrease in frequency of optical modes from Ga$_2$SO to Ga$_2$TeO due to increasing atomic mass is noticed.

To further verify the structural stability at high temperatures, we perform *ab initio* molecular dynamics simulations by using the microcanonical ensemble. Size constraint is altered by constructing a $6 \times 6 \times 1$ supercell and total simulation time is set to 3 ps with 1-fs time steps for varying temperatures. As seen from the snapshots in Fig. 2(b), no significant distortions are noticed for Ga$_2$SO and Ga$_2$SeO up to 600 K, confirming the dynamical stability. On the other hand, the crystal structure of Ga$_2$TeO is deformed even at 300 K in parallel with the phonon spectrum results. Additionally Ga-Te bonds start to be broken at higher temperatures, indicating structural decomposition. Even though these results do not
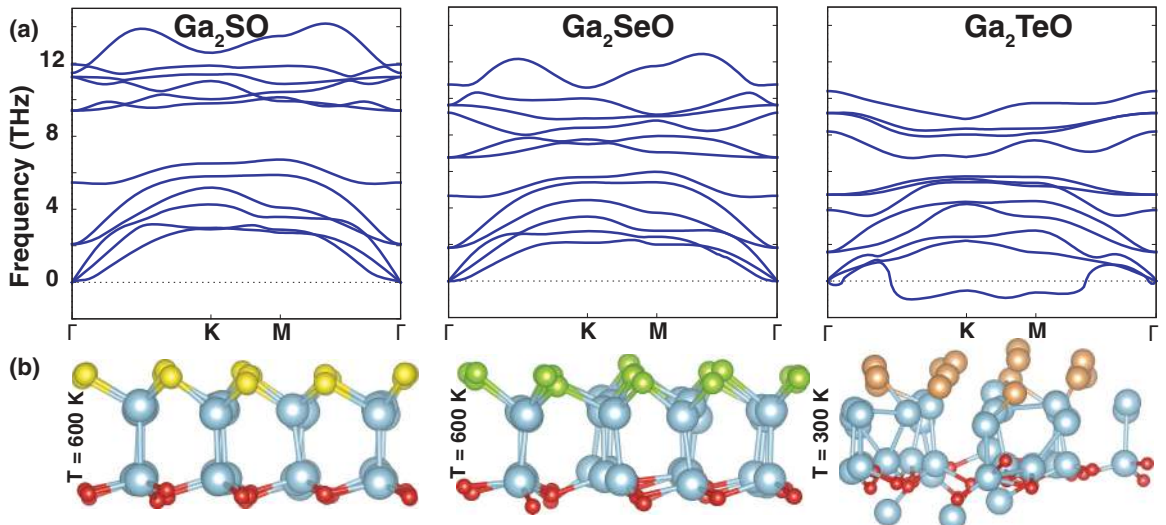

FIG. 2. (a) Phonon band structures and (b) snapshots of *ab initio* molecular dynamics simulations of Ga$_2$SO, Ga$_2$SeO, and Ga$_2$TeO monolayers.

TABLE II. The variation of electronic band gaps at the level of PBE with strain in eV. Metallic systems are denoted with M.

	$E_{\text{gap}}^{\text{PBE}}$ (eV)								
	−6%	−4%	−2%	0%	+2%	+4%	+%6	+8%	+10%
Ga$_2$SO	1.41	1.30	1.15	1.28	0.71	0.46	0.22	0.01	M
Ga$_2$SeO	M	M	0.01	0.39	0.75	1.10	1.32	1.24	1.11
Ga$_2$TeO	M	M	M	M	M	M	0.02	0.42	0.74

totally exclude possible stable structures with long-range order, it can be concluded that oxygenation of monolayer GaTe makes the system unstable. The instability can be correlated to asymmetric charge transfer from Ga to O and Te atoms. As discussed above, while O accepts $0.94e$, charge donated to Te is only $0.30e$. This not only weakens Ga-Te bonds but also affects Ga-Ga bonds. $d_{\text{Ga-Ga}}$ in GaTe elongated from 2.46 to 2.54 Å in Ga$_2$TeO results in dynamical instability.

B. Mechanical properties

Revealing the structural stability, first mechanical properties of Ga$_2X$O monolayers are studied. Mechanical response of 2D systems is not only a critical factor for their integration into devices but also affects their performance [2]. The elastic properties can be obtained once the relevant elastic constants are determined. For Ga$_2X$O monolayers, all elastic constants (C_{ij}) are found to be positive, satisfying the Born stability criteria [45]. The in-plane stiffness (Y_{2D}) and Poisson's ratio (ν) are then calculated by using the following relations, $Y_{\text{2D}} = (C_{11}^2 - C_{12}^2)/C_{11}$ and $\nu = C_{12}/C_{11}$, and results are summarized in Table I. In parallel with elongation of bond lengths, Y_{2D} (and also bulk modulus, Y) decreases down the chalcogen group. As GaO has the highest Y_{2D} among GaX monolayers, the inclusion of O increases Y_{2D} of Ga$_2$SO and Ga$_2$SeO when compared to GaS and GaSe, making them more rigid. The decrease in Y_{2D} of Ga$_2$TeO can be explained
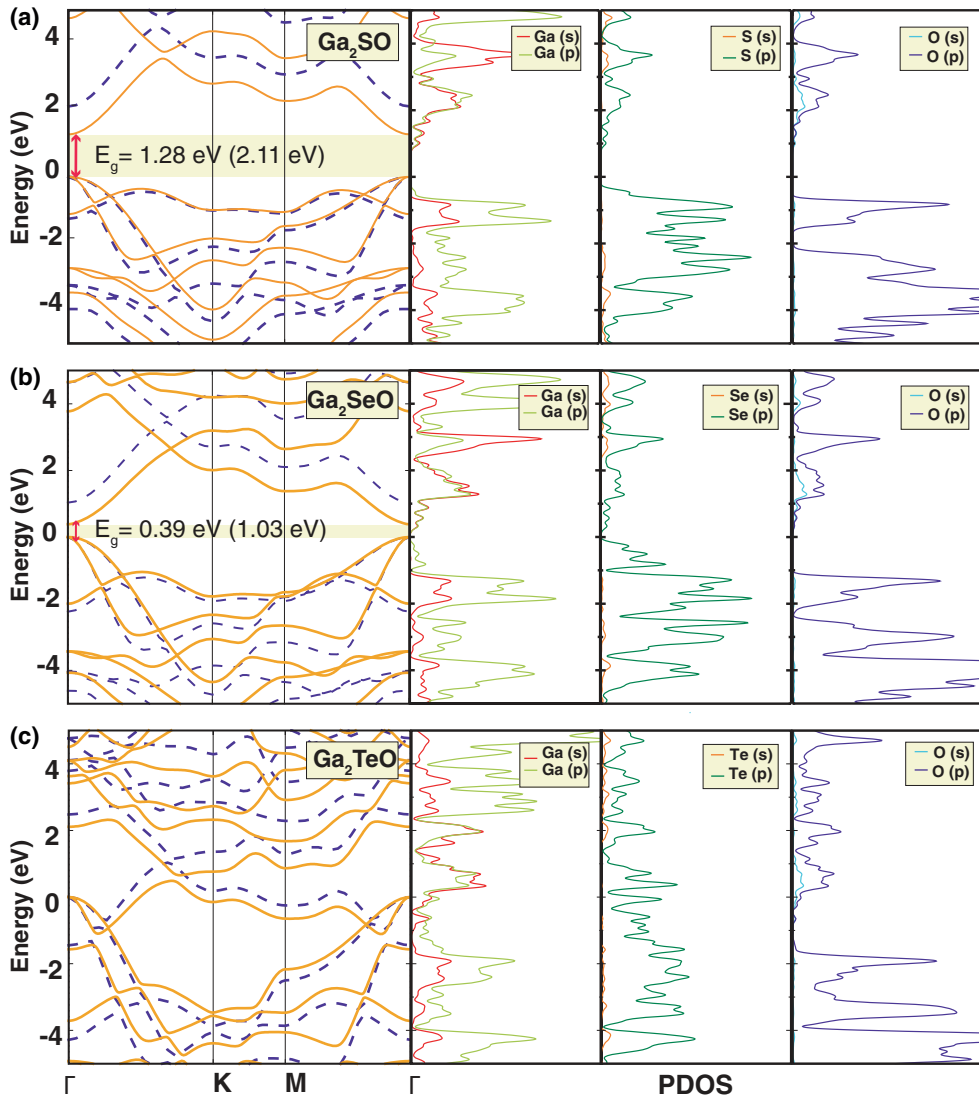

FIG. 3. The electronic band structures and projected density of states (PDOS) of (a) Ga$_2$SO, (b) Ga$_2$SeO, and (c) Ga$_2$TeO monolayers. GGA-PBE and HSE06 results are shown by orange solid and blue dashed lines, respectively. E_g at the level of PBE (HSE06) is also shown. The Fermi level is set to zero.
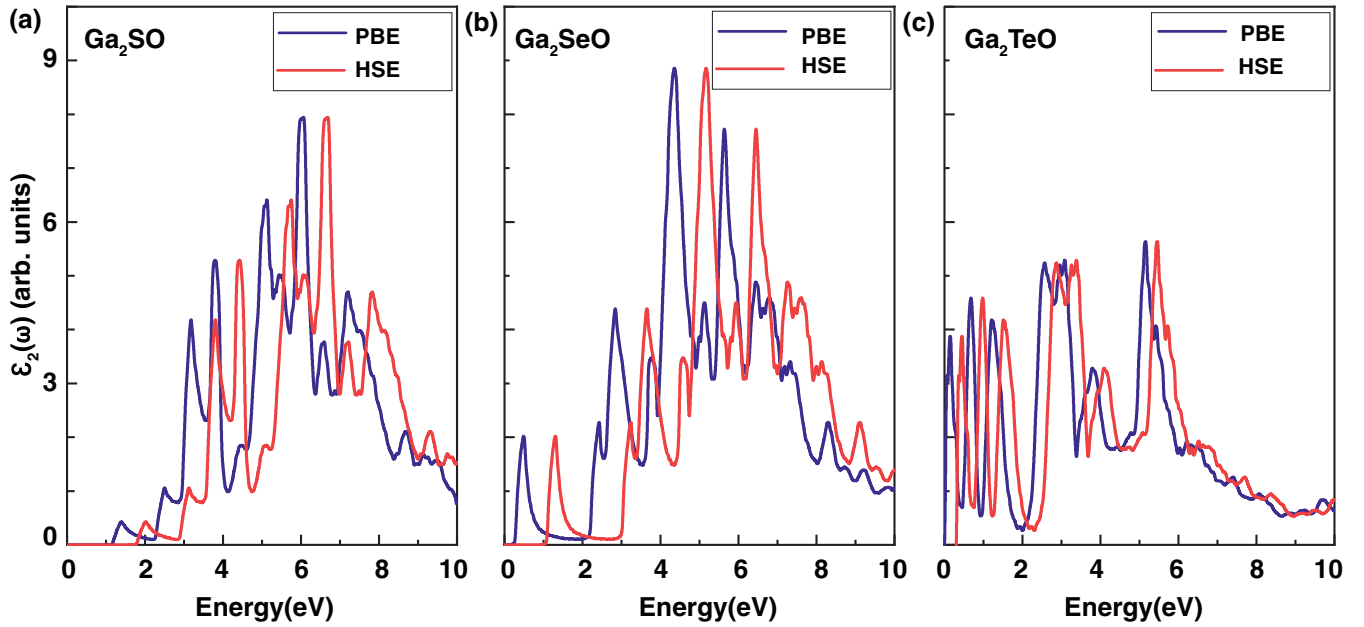
FIG. 4. The variation of the imaginary part of the dielectric function [$\epsilon_2(\omega)$] with photon energy for in-plane polarization for (a) Ga$_2$SO, (b) Ga$_2$SeO, and (c) Ga$_2$TeO monolayers.

with the instability of the structure. Next, Poisson's ratio (ν), which is the ratio of the transverse strain to the axial strain ($\nu = -\epsilon_{\text{trans}}/\epsilon_{\text{axial}}$), is calculated and it is found that ν increases down the chalcogen group. Smaller ν indicates a stronger degree of covalent bonding resulting in higher hardness. Based on Frantsevich's criteria [46], while GaS ($\nu = 0.24$) and GaSe ($\nu = 0.24$) are brittle, GaO ($\nu = 0.38$) is ductile [14]. In parallel with this trend Ga$_2$SO ($\nu = 0.30$) and Ga$_2$SeO ($\nu = 0.32$) are at the boundary of ductile and brittle character (i.e., oxygenation makes these systems less brittle). For the sake of completeness, ν of Ga$_2$TeO is also calculated and is found to be 0.39. Apart from instability issues, a higher ν value is expected for Ga$_2$TeO because of its metallic character.

C. Electronic properties

Electronic band structures of Ga$_2X$O monolayers are calculated at the level of GGA-PBE and HSE06 along the high-symmetry points of Γ-K-M-Γ as shown in Fig. 3. While the binary constituents (GaO, GaS, and GaSe) have indirect band gaps, addition of O atoms as a third component makes ternary Ga$_2$SO and Ga$_2$SeO direct band-gap (E_g) semiconductors with E_g^{PBE} of 1.28 and 0.39 eV, respectively, and both the valence-band maximum (VBM) and conduction-band minimum (CBM) locate at the Γ point. As discussed above, the lattice constant of Ga$_2X$O lies between those of GaX and GaO. Therefore, while the O side of Ga$_2X$O is exposed to tensile strain, the X side experiences a compressive strain. The exposure of anisotropic strain induces indirect-direct band-gap transition. A similar effect is also obtained for ternary In$_2$SSe and MoXY monolayers [23,47]. Additionally, following the formation of ordered alloy upon oxygenation, E_g of Ga$_2X$O monolayers are smaller than those of binary systems and E_g decreases down the chalcogen group and even makes Ga$_2$TeO metallic. When calculations are repeated using the

HSE06 hybrid functional, as expected larger E_g are obtained but the band-structure profiles are not modified. The metallic character of Ga$_2$TeO is also preserved. It should be noted that the electronic structure of the Ga$_2$TeO monolayer is related with the suggested geometry and metallicity can be altered in a different structure with long-range order.

When projected densities of states of Ga$_2X$O are analyzed (Fig. 3), it is noticed that mainly hybridization between Ga-s, Ga-p, X-p, and O-p orbitals contributes to the levels just below/above the Fermi level (corresponding to the VBM and CBM for semiconducting systems), which is similar to their GaX constituents. Different from other GaX monolayers, GaO has a distinct VBM composed of Ga-s, Ga-p, and O-p orbitals [14], which leads to band-gap narrowing in Ga$_2X$O ternary structures.

D. Strain dependent electronic properties

In addition to inherent strain on both sides of Ga$_2X$O monolayers, we also analyze the variation of electronic band structure under biaxial strain. Strain engineering is a promising strategy to tune electronic performance of 2D materials and offers new opportunities for device applications [48]. In this respect tensile (compressive) strain up to $+10\%$ (-6%) is applied. For each strain level, the geometries are reoptimized and then the band structures are calculated. Obtained band gaps are summarized in Table II. For Ga$_2$SO, E_g gradually decreases with tensile strain and the system becomes metallic around $\approx 10\%$. On the other hand E_g gradually increases with compressive strain and becomes 1.41 eV at -6%. For both tensile and compressive strain, direct to indirect band-gap transition is noticed. The response of Ga$_2$SeO is different from Ga$_2$SO. First, E_g increases with tensile strain up to 6% preserving the direct character and then decreases (and also becomes indirect) at higher strain levels as plastic deformation starts. For compressive strain, E_g decreases and
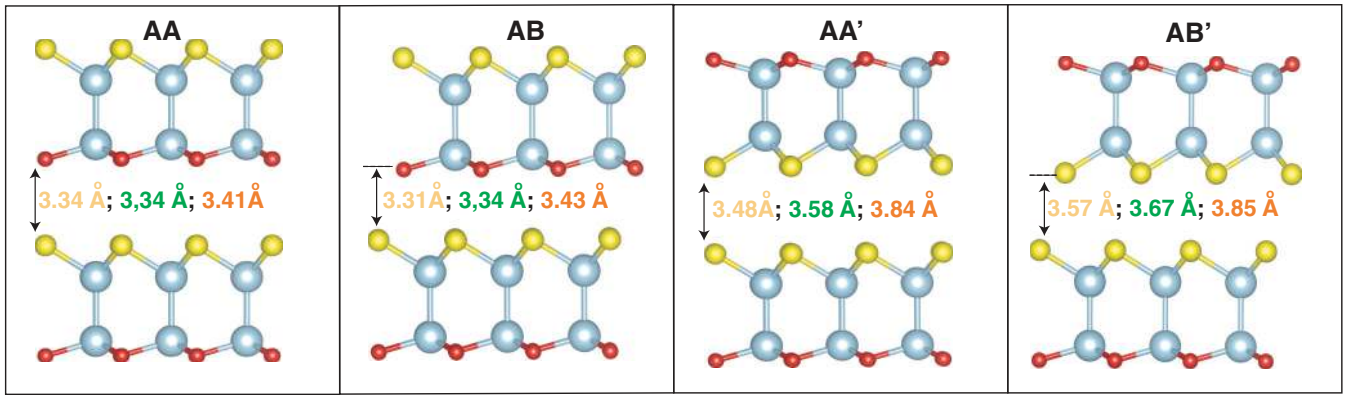
FIG. 5. The side views of Ga_2XO bilayers for AA, AB, AA', and AB' stacking orders. Ga, X, and O atoms are shown with blue, yellow, and red spheres, respectively. The interlayer distance for Ga_2SO, Ga_2SeO, and Ga_2TeO is given by yellow, green, and orange colors, respectively.

Ga_2SeO becomes metallic after -2%. The different response between the two materials can be correlated with the variation of local potential on O and X atomic layers [the (x,y)-plane averaged electronic potential profile along with the z axis for the unstrained case is presented in Supplemental Material [40]]. Considering the O layer as a reference, while the potential difference between O- and S-atomic layers increases in Ga_2SO with tensile strain, the potential difference between O- and Se-atomic layers decreases and becomes negative in Ga_2SeO. For Ga_2TeO, the system remains metallic under compressive strain but metal to semiconductor transformation occurs at 6% and then E_g widens with increasing compressive strain.

E. Optical properties

Finally, the optical response of Ga_2XO monolayers is studied by obtaining the frequency dependent complex dielectric function $[\epsilon(\omega) = \epsilon_1(\omega) + i\epsilon_2(\omega)]$, which enables calculation of the optical properties (i.e., absorbance, optical conductivity, absorption coefficient, and reflectivity). The variation of $\epsilon_2(\omega)$ with photon energy for in-plane light polarization is given in Fig. 4. Based on HSE06 results, for Ga_2SO the onset of absorption is at 2.1 eV in accordance with the direct electronic band gap, and main absorption peaks remain in the visible and near-UV region. Interestingly, for Ga_2SeO the absorption onset is in the infrared regime (≈ 1 eV) and the second peak remains in the near-UV region (≈ 3.5 eV) and there is almost no absorption in the visible spectrum. This characteristic can be used in design of visible-blind detectors which can operate both in the UV and IR region. As Ga_2TeO is metallic, strong

absorption is noticed at low energy levels due to intraband transitions (Drude term) and the next strong peak suggests significant light absorption in the visible and near-UV region.

F. Bilayer structures

In the last part, in addition to monolayers, the bilayers of Ga_2XO for all possible stackings are explored. As illustrated in Fig. 5, for AA stacking order, the top layer is exactly on top of the bottom layer; for AB stacking, the top layer is shifted so that O atoms are on the hexagon center of the bottom layer; for the AA' stacking, the inverted top layer is exactly on top of the bottom layer; and for AB' stacking, the inverted top layer is shifted so that X atoms are on the hexagon center of the bottom layer. For the sake of completeness, the calculations are also repeated for Ga_2TeO, the monolayer of which is found to be unstable. For all stacking orders the interlayer distance is between 3.34 and 3.85 Å (Fig. 5) and the interlayer interaction energy (E_{int}) is between 0.14 and 0.31 eV (Table III), indicating vdW interactions between monolayers. Onset of chemical bonding between layers is not noticed. When total energies are compared, the ground-state configuration is AB stacking for Ga_2SO and AB' for Ga_2SeO and Ga_2TeO, but the energy difference (ΔE) between them is less than 10 meV/cell for all systems. However small ΔE is, stacking order alters the E_g as shown in Fig. 6. The highest (lowest) E_g is obtained for AA (AB) stacking. For semiconducting systems, E_g of bilayers is smaller than monolayers due to quantum confinement but the direct character is preserved. Also, it should be noted that bilayer Ga_2TeO remains metallic for all configurations.

TABLE III. The interaction energy between monolayers E_{int}, the energy difference between different stackings ΔE, and the energy band gap at the level of PBE (E_g^{PBE}) and HSE06 (E_g^{HSE}). All energies are given in eV.

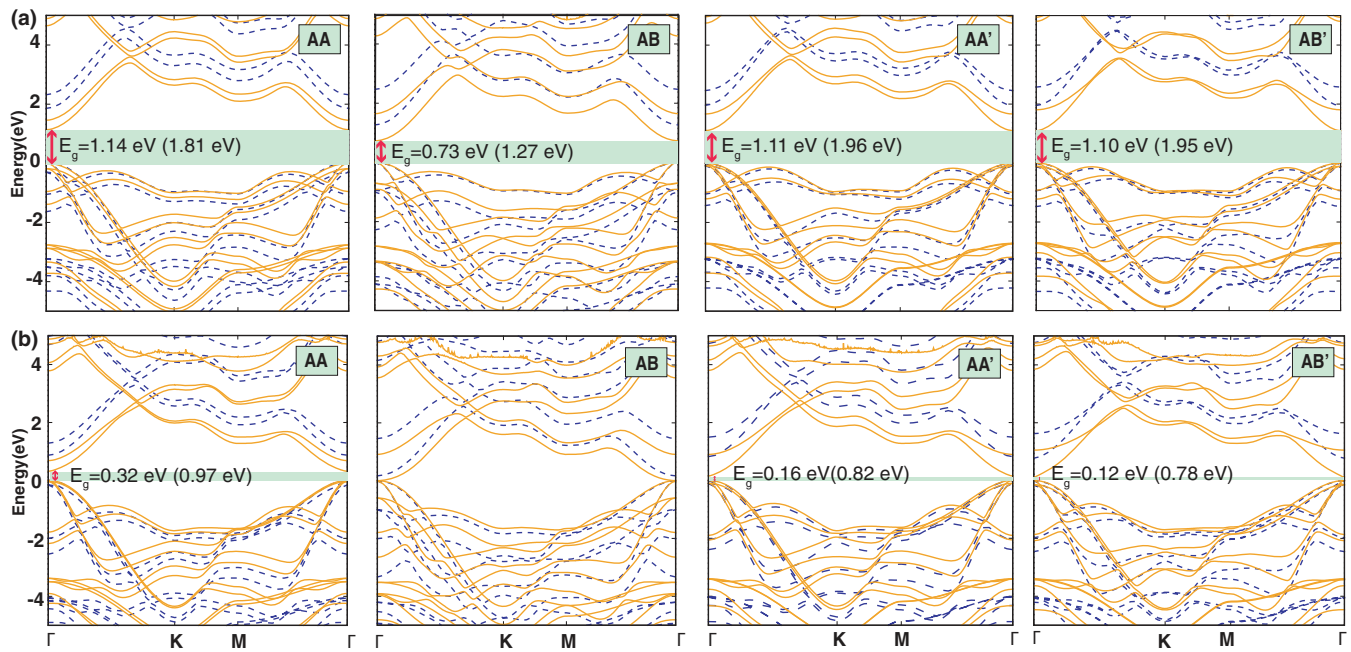|	AA				AB				AA'				AB'			
	E_{int}	ΔE	E_g^{PBE}	E_g^{HSE}	E_{int}	ΔE	E_g^{PBE}	E_g^{HSE}	E_{int}	ΔE	E_g^{PBE}	E_g^{HSE}	E_{int}	ΔE	E_g^{PBE}	E_g^{HSE}
Ga_2SO	-0.138	0.08	1.14	1.81	-0.216		0.73	1.28	0.150	0.07	1.11	1.96	-0.213	0.01	1.10	1.95
Ga_2SeO	-0.155	0.10	0.32	0.87	-0.246	0.01	M	0.17	-0.178	0.08	0.16	0.82	-0.255		0.12	0.78
Ga_2TeO	-0.186	0.12	M	M	-0.300	0.01	M	M	-0.225	0.08	M	M	-0.305		M	M

FIG. 6. The electronic band structures of (a) Ga_2SO and (b) Ga_2SeO bilayers for different stackings. GGA-PBE and HSE06 results are shown by orange solid and blue dashed lines, respectively. E_g at the level of PBE (HSE06) is also shown.

IV. CONCLUSION

In summary, we examined the fundamental properties of 2D Ga_2XO ($X = $ S, Se, Te) systems which can be realized by partial oxygenation. Vibrational frequency analysis and molecular dynamics simulations revealed that while Ga_2SO and Ga_2SeO are stable even at high temperatures Ga_2TeO is dynamically unstable. The inclusion of oxygen decreases (increases) in-plane stiffness (Poisson's ratio) of Ga_2XO monolayers making them less brittle when compared to their binary constituents. While GaX monolayers have indirect band gaps, Ga_2SO and Ga_2SeO become direct band-gap semiconductors due to induced asymmetric strain on both sides. The obtained band gaps and indirect-direct transition can be further controlled by applied strain. While Ga_2SO has strong optical absorption in the visible region, main peaks of Ga_2SeO remain in the infrared and ultraviolet region, making it visible blind. Finally, in addition to monolayers, bilayers are considered and it is shown that bilayers of Ga_2XO can be formed by van der Waals interaction, which indicates the possibility of tuning electronic properties with number of layers and stacking order. Our results not only predict stable 2D ternary Ga_2XO structures but also suggest them as promising materials for optoelectronic applications due to their enhanced mechanical, electronic, and optical properties.

[1] H. Zhang, M. Chhowalla, and Z. Liu, Chem. Soc. Rev. **47**, 3015 (2018).

[2] D. Akinwande, C. J. Brennan, J. S. Bunch, P. Egberts, J. R. Felts, H. Gao, R. Huang, J.-S. Kim, T. Li, Y. Li *et al.*, Extreme Mech. Lett. **13**, 42 (2017).

[3] A. J. Mannix, B. Kiraly, M. C. Hersam, and N. P. Guisinger, Nat. Rev. Chem. **1**, 0014 (2017).

[4] W. Huang, L. Gan, H. Li, Y. Ma, and T. Zhai, Cryst. Eng. Comm. **18**, 3968 (2016).

[5] S. Yang, Y. Li, X. Wang, N. Huo, J.-B. Xia, S.-S. Li, and J. Li, Nanoscale **6**, 2582 (2014).

[6] A. Harvey, C. Backes, Z. Gholamvand, D. Hanlon, D. McAteer, H. C. Nerl, E. McGuire, A. Seral-Ascaso, Q. M. Ramasse, N. McEvoy *et al.*, Chem. Mater. **27**, 3483 (2015).

[7] P. Hu, L. Wang, M. Yoon, J. Zhang, W. Feng, X. Wang, Z. Wen, J. C. Idrobo, Y. Miyamoto, D. B. Geohegan *et al.*, Nano Lett. **13**, 1649 (2013).

[8] P. Hu, Z. Wen, L. Wang, P. Tan, and K. Xiao, ACS Nano **6**, 5988 (2012).

[9] S. Lei, L. Ge, Z. Liu, S. Najmaei, G. Shi, G. You, J. Lou, R. Vajtai, and P. M. Ajayan, Nano Lett. **13**, 2777 (2013).

[10] Z. Wang, K. Xu, Y. Li, X. Zhan, M. Safdar, Q. Wang, F. Wang, and J. He, ACS Nano **8**, 4859 (2014).

[11] F. Liu, H. Shimotani, H. Shang, T. Kanagasekaran, V. Zólyomi, N. Drummond, V. I. Fal'ko, and K. Tanigaki, ACS Nano **8**, 752 (2014).

[12] W. Feng, X. Zhou, W. Q. Tian, W. Zheng, and P. Hu, Phys. Chem. Chem. Phys. **17**, 3653 (2015).

[13] M. Wu, J.-j. Shi, M. Zhang, Y.-m. Ding, H. Wang, Y.-l. Cen, and J. Lu, Nanoscale **10**, 11441 (2018).

[14] S. Demirci, N. Avazlı, E. Durgun, and S. Cahangirov, Phys. Rev. B **95**, 115409 (2017).

[15] G. Shen, D. Chen, P.-C. Chen, and C. Zhou, ACS Nano **3**, 1115 (2009).

[16] Y. Ma, Y. Dai, M. Guo, L. Yu, and B. Huang, Phys. Chem. Chem. Phys. **15**, 7098 (2013).

[17] H. L. Zhuang and R. G. Hennig, Chem. Mater. **25**, 3232 (2013).

[18] W. Wei, Y. Dai, C. Niu, X. Li, Y. Ma, and B. Huang, J. Mater. Chem. C **3**, 11548 (2015).

[19] S. Zhou, C.-C. Liu, J. Zhao, and Y. Yao, npj Quantum Mater. **3**, 16 (2018).

[20] T. E. Beechem, B. M. Kowalski, M. T. Brumbach, A. E. McDonald, C. D. Spataru, S. W. Howell, T. Ohta, J. A. Pask, and N. G. Kalugin, Appl. Phys. Lett. **107**, 173103 (2015).

[21] A.-Y. Lu, H. Zhu, J. Xiao, C.-P. Chuu, Y. Han, M.-H. Chiu, C.-C. Cheng, C.-W. Yang, K.-H. Wei, Y. Yang *et al.*, Nat. Nanotechnol. **12**, 744 (2017).

[22] J. Zhang, S. Jia, I. Kholmanov, L. Dong, D. Er, W. Chen, H. Guo, Z. Jin, V. B. Shenoy, L. Shi *et al.*, ACS Nano **11**, 8192 (2017).

[23] A. Kandemir and H. Sahin, Phys. Rev. B **97**, 155410 (2018).

[24] Y. Guo, S. Zhou, Y. Bai, and J. Zhao, Appl. Phys. Lett. **110**, 163102 (2017).

[25] H. D. Bui, H. R. Jappor, and N. N. Hieu, Superlattices Microstruct. **125**, 1 (2019).

[26] G. Kresse and J. Hafner, Phys. Rev. B **47**, 558 (1993).

[27] G. Kresse and J. Hafner, Phys. Rev. B **49**, 14251 (1994).

[28] G. Kresse and J. Furthmüller, Comput. Mater. Sci. **6**, 15 (1996).

[29] G. Kresse and J. Furthmüller, Phys. Rev. B **54**, 11169 (1996).

[30] J. P. Perdew, K. Burke, and M. Ernzerhof, Phys. Rev. Lett. **77**, 3865 (1996).

[31] P. E. Blöchl, Phys. Rev. B **50**, 17953 (1994).

[32] H. J. Monkhorst and J. D. Pack, Phys. Rev. B **13**, 5188 (1976).

[33] D. Pines and D. Bohm, Phys. Rev. **85**, 338 (1952).

[34] P. Cudazzo, I. V. Tokatly, and A. Rubio, Phys. Rev. B **84**, 085406 (2011).

[35] L. C. Gomes and A. Carvalho, Phys. Rev. B **92**, 085406 (2015).

[36] T. C. Berkelbach, M. S. Hybertsen, and D. R. Reichman, Phys. Rev. B **88**, 045318 (2013).

[37] K. Noori, N. L. Q. Cheng, F. Xuan, and S. Y. Quek, 2D Mater. **6**, 035036 (2019).

[38] J. Neugebauer and M. Scheffler, Phys. Rev. B **46**, 16067 (1992).

[39] M. Otani and O. Sugino, Phys. Rev. B **73**, 115407 (2006).

[40] See Supplemental Material at http://link.aps.org/supplemental/10.1103/PhysRevB.101.075423 for the (x,y)-plane averaged electronic potential profile along with z axis for monolayers of Ga_2SO, Ga_2SeO, and Ga_2TeO.

[41] A. Togo and I. Tanaka, Scr. Mater. **108**, 1 (2015).

[42] J. Paier, M. Marsman, K. Hummer, G. Kresse, I. C. Gerber, and J. G. Ángyán, J. Chem. Phys. **124**, 154709 (2006).

[43] S. Grimme, J.Comput. Chem. **27**, 1787 (2006).

[44] G. Henkelman, A. Arnaldsson, and H. Jónsson, Comput. Mater. Sci. **36**, 354 (2006).

[45] F. Mouhat and F.-X. Coudert, Phys. Rev. B **90**, 224104 (2014).

[46] I. Frantsevich, F. Voronov, and S. Bokuta, *Elastic Constants and Elastic Moduli of Metals and Insulators Handbook* (Naukova Dumka, Kiev, Ukraine, 1983), pp. 60–180.

[47] M. Yagmurcukardes, C. Sevik, and F. M. Peeters, Phys. Rev. B **100**, 045415 (2019).

[48] Z. Dai, L. Liu, and Z. Zhang, Adv. Mater. **31**, 1805417 (2019).